phys. stat. sol. (a) **186**, No. 3, 493–503 (2001)

Analysis of a Hot Electron Light Emitting Device at Low and High Electric and Magnetic Fields

A. TEKE

Department of Physics, Faculty of Art and Science, Baikesir University, Baikesir, Turkey

(Received December 20, 2000; in revised form May 21, 2001; accepted May 21, 2001)

Subject classification: 72.20.Fr; 72.20.Ht; 73.40.Kp; 78.60.Fi; S7.12

The electrical characterization of a tunable wavelength surface light-emitting device is reported. The device consists of p-GaAs and n-$Ga_{1-x}Al_xAs$ heterojunction containing an inversion layer on the p-side, and GaAs quantum wells on the n-side, and is referred to as HELLISH-2 (Hot Electron Light Emitting and Lasing in Semiconductor Heterojunction). We studied two HELLISH-2 devices by using standard Hall, SdH (Shubnikov de Haas) and high-speed I–V measurement techniques. 2D carrier density and transport mobility were obtained from standard Hall measurements and quantum lifetime and quantum mobility were determined from SdH measurements. A detailed analysis of the results has been performed to understand the scattering processes involved in device operation. We have concluded that a good knowledge of electrical parameters is important in order to optimize the device structures based on our model calculations.

1. Introduction

A hot electron light emitter, HELLISH-2 (Hot Electron Light Emitting and Lasing in Semiconductor Heterojunction-type 2) that can be operated in either single or multiple wavelength emission has been developed and reported by us [1, 2]. In this paper, we present the electrical properties of HELLISH-2 and scattering process involved in device operation at low and high electric and magnetic fields by using standard Hall, SdH and I–V measurement techniques. These are the most common characterization techniques used in semiconductor assessment. Experimental data obtained from these measurements over a wide temperature (4.2–300 K) and electric (few V/m–kV/m) and magnetic (0.3–6 T) field ranges gives information on carrier mobilities and densities, quantum mobilities and quantum lifetime, impurities, parallel conduction, scattering mechanism, etc. [3]. Classical transport and magnetotransport are characterized by transport or Hall mobility. The SdH effect is characterized by the quantum lifetime. The quantum lifetime τ_q is defined as the mean time between two successive scattering events. It is inversely proportional to the scattering rate, regardless of the scattering angle. The quantum lifetime defines a quantum mobility as $\mu_q = e\tau_q/m^*$. Transport or Hall mobility μ_{Hall} in contrast is determined by the momentum transfer in the direction of the electric field, and the contribution of each scattering event to the electrical transport depends therefore on the scattering angle. The ratio of μ_q/μ_{Hall} depends on the mean scattering angle. The contribution of both electrons with a small and a large mean scattering angle to the quantum mobility is identical but electron has a much higher contribution to electrical transport for the small-angle scattering. Such information on transport parameters are important for the improvement of growth parameters used to prepare high quality epitaxial layers and also for device applications. The parameters obtained from these measurements are also used in our model, which is developed by us [2] to understand the device operation and optimize the structure for higher performances.

 0031-8965/01/18608-0493 $ 17.50+.50/0

2. Structures and Operation Principle of HELLISH-2

The samples, coded as ES1 and ES2 were grown on Cr-doped semi-insulating GaAs substrates oriented in the ⟨100⟩ direction by MBE. Together with their band edge profile, Fig. 1 shows the schematic representation of the structure of ES1 and ES2. The substrate temperature was kept constant at 580 ºC during the growth of all epilayers. For ES2 the layer sequence starts with the growth of a 4 μm thick undoped GaAs buffer layer on top of the SI substrate. Although the buffer layer is intended to be intrinsic, it turned out to be p-type probably due to carbon impurities. For sample ES1 the GaAs buffer layer is intentionally p-doped by Be with a doping density $N_A \approx 5 \times 10^{16}$ cm^{-3}. For both samples, the rest of the structure is identical. The buffer layer is followed by a set of ten periods of GaAs quantum wells with 75 Å well width. The $Ga_xAl_{1-x}As$ barriers with an Al content of $x = 33\%$ consist of a 75 Å thick Si-doped layer with a doping density $N_D \approx 8 \times 10^{17}$ cm^{-3} sandwiched between two 110 Å undoped spacer layers. A 225 Å thick Si-doped ($N_D \approx 8 \times 10^{17}$ cm^{-3}) $Al_{0.33}Ga_{0.67}As$ layer was grown on top of this ten-periodic multiple quantum wells and the growth is completed by growing a 240 Å thick undoped GaAs capping layer to prevent oxidation of the $Al_{0.33}Ga_{0.67}As$ layers.

Figure 2 shows the schematics of the carrier dynamics involved in device operation. When the electric field is applied parallel to the layers, the electrons in the quantum well adjacent to the junction plane are heated up to non-equilibrium temperatures $T_{e1} > T_L$ and transferred to the inversion layer via phonon-assisted tunnelling and thermionic emission. In the case of thermionic emission electrons being transferred over the barrier from quantum well to inversion layer ballistically and in the case of phonon-assisted tunneling process, electrons are injected from quantum well to the inversion layer by absorption of an optical phonon. The accumulation of excess negative charge in the inversion layer via these two processes modifies the potential profile where the depletion region on the p-side of the junction is decreased so that the p-side of the depletion region behaves as forward biased. Therefore, the holes which are initially away from the junction diffuse towards the junction plane. Thus, the electron and hole wave functions overlap in the vicinity of the inversion layer giving rise to a radiative recombination ($h\nu_1$), which corresponds to band-to-band transition in GaAs. As the

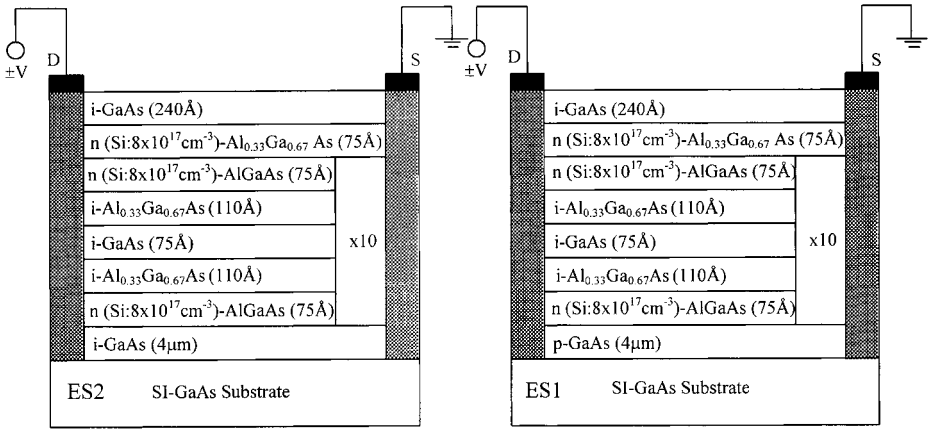

Fig. 1. Layered structure of the samples ES1 and ES2

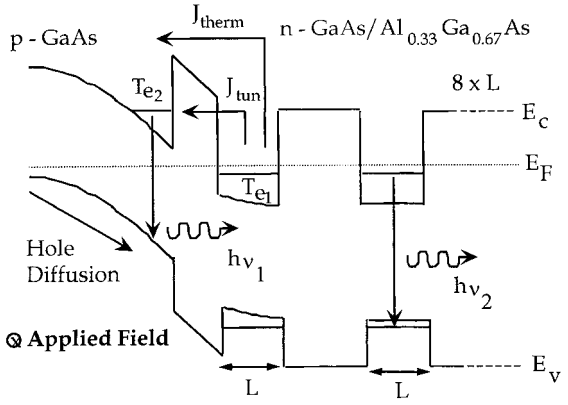

Fig. 2. Schematic illustration of the carrier dynamics involved in device operation of HELLISH-2. T_{e1} and T_{e2} are the electron temperatures in the quantum well and in the inversion layer, respectively. J_{ther} and J_{tun} are the thermionic and tunnelling components of the hot electron currents from quantum well to the inversion layer, respectively. L is the first quantum well widths. Electric field is applied parallel to the layers

field is increased injected hot electron current from quantum well to the inversion layer increases. Furthermore, the non-equilibrium electrons in the inversion layer, which also see the same external field, heat up to a temperature $T_{e2} > T_L$ and occupy the higher energy states according to their Fermi-Dirac distribution. Therefore, a high energy tail which is representative of a Maxwellian distribution is expected to develop in the spectra associated with the inversion layer transition. However, since the emitted light is collected from the surface of the samples, photons from the inversion layer with energies greater than the e1–hh1 energy separation in the quantum wells will be absorbed by the quantum well and re-emitted at energy $h\nu_2$ corresponding to the e1–hh1 transition in the well. With increasing field, both the injected hot electron density in the inversion layer and the occupancy of high-energy states increases, so that more high-energy photons become available for absorption in the wells. Moreover, since the holes in the p-layer are subjected to the same electric field, hot holes are diffused into the quantum well where they recombine radiatively with the electrons. As a result, the intensity of re-emission from the quantum wells increases rapidly with increasing field for all samples. Electroluminesence and photoluminesence spectra of sample ES1 and a theoretical model developed to understand the device operation were published elsewhere [1, 2]. These works, realizing a reasonable good agreement between experimental results and our model led us to increase the device performance by optimizing the structural parameters. In modelling (calculation of the potential profile of the device and calculation of injected current density via thermionic emission and phonon-assisted tunnelling) the doping concentration in the n- and p-sides of the heterojunction, the barrier width between the inversion layer and quantum well, quantum well width and Fermi level outside the depletion region are used as input parameters. Therefore, a good knowledge of some of these parameters obtained from Hall and SdH measurements is important for optimization processes using our model. The output parameters yielded from these model calculations are the quantized energy levels both in inversion layer and quantum well, the depletion length of both sides of the heterojunction and 2D electron concentration in the well and the inversion layer.

3. Experimental Results

The samples ES1 and ES2 were characterized electrically by Hall and van der Pauw measurement techniques at low fields. The dimensions of the samples were typically

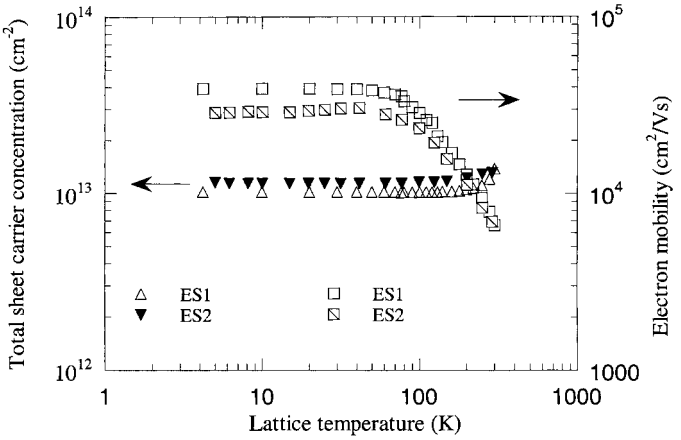

Fig. 3. Total sheet electron density and Hall mobility as a function of lattice temperature obtained from Hall and van der Pauw measurement techniques for samples ES1 and ES2, respectively

3.5×1.75 mm^2 and 4×4 mm^2 for Hall bar and cloverleaf shapes, respectively. Ohmic contacts were formed by diffusing Ni/AuGe/Ni/Au for Hall bar samples and Sn for cloverleaf samples into the structures. Both measurements were carried out in a lattice temperature range between 4.2 and 300 K in darkness. The temperature dependence of Hall mobility and sheet electron concentration for all samples is shown in Fig. 3.

As seen from this figure both samples show almost the same characteristics. The electron densities remain constant up to a lattice temperatures of 140 K for samples ES1 and ES2. However, above these temperatures the electron concentrations increase monotonically with lattice temperature for both samples probably because of temperature-induced thermal excitation of impurities (Si) in the $Al_{0.33}Ga_{0.67}$ As region [4, 5]. Activation energy E_a of 11.0 and 8.2 meV, which are in agreement with the donor ionization energies of the $Ga_xAl_{1-x}As$ structures [6] were obtained for the samples ES1 and ES2, respectively. The flat region below this temperature implies that the conduction is dominated almost exclusively by the carriers in the wells. The parallel conducting channel (such as the p-type GaAs buffer layer and electrons in the undepleted $Al_{0.33}Ga_{0.67}As$ barriers) contributing to the major conduction channel in the wells will be discussed later during the analysis of the van der Pauw results of selectively etched samples and SdH results.

Electron mobility remains almost constant from 4.2 up to 40 K for sample ES1. For ES2, it increases slightly with increasing lattice temperature up to 40 K, but this increase is not monotoneously, and only 5% within the temperature range. Therefore, electron mobilities for both samples can be considered constant within the experimental accuracy and are probably determined by combination of both interface roughness and background impurity scattering. The reasons why the dominant mechanisms are interface roughness and background impurity scattering are the following: (i) in inverted heterostructures and quantum well structures the interface between $Al_xGa_{1-x}As$ and GaAs is very poor. Only a small roughness of heterointerface can cause a large fluctuation in the quantization of energy of confined 2D electrons, which would lead to a very strong momentum scattering [7]. It has also been reported that background impurity

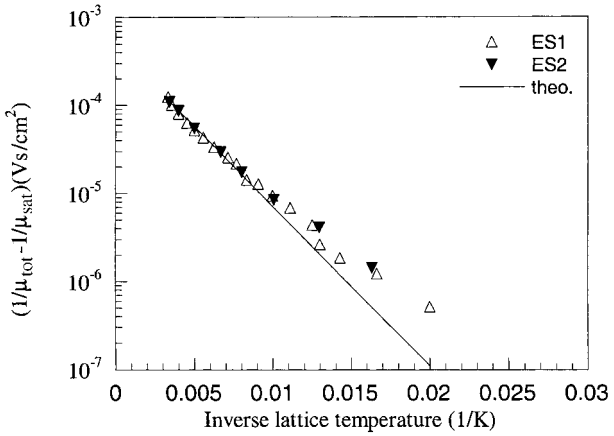

Fig. 4. Inverse of optic phonon-limited electron mobility versus inverse lattice temperature for samples ES1 and ES2. The solid line is drawn by taking $\hbar\omega$ = 36 meV in Eq. (1)

scattering arising from dopant (Si) segregation from doped $Al_xGa_{1-x}As$ into the GaAs quantum well interface is quite significant in inverted and quantum well structures with a thin spacer layer at a growth temperature of around 580 °C [8]. Since the momentum relaxation rate for background impurity scattering has the same energy dependence as that of remote impurity scattering rate, both scattering mechanisms (interface roughness and background impurity scattering) saturate the mobility at low temperatures ($T_L < 40$ K) as observed in the present samples; and (ii) the magnitude of the observed mobility is much lower than would result from remote impurity scattering and in the same range as that expected from the interface roughness and background impurity scattering [7, 8]. At high temperatures $T_L > 40$ K, however, mobility for all the samples decreases gradually with increasing temperature as shown in Fig. 3. In order to obtain the dominant scattering mechanism that limits the mobility at high temperatures we used Matthiesen's rule. The result is shown in Fig. 4 where the logarithm of the difference between the inverse of total and saturation mobilities (low temperature mobilities) are plotted against inverse lattice temperature. The line is well described by a scattering mechanism involving LO phonons [9],

$$\left(\frac{1}{\mu_{tot}}-\frac{1}{\mu_{sat}}\right) \propto \exp\left(-\frac{\hbar\omega}{k_B T_L}\right), \tag{1}$$

where $\hbar\omega$ is the LO phonon energy and k_B the Boltzmann constant. Therefore, the slope of the line gives the LO phonon energy, $\hbar\omega$ = 36 meV. Deviation at low temperatures can be attributed to the contribution of other scattering mechanisms or enhanced errors in the calculation of $(1/\mu_{tot}-1/\mu_{sat})$ due to the very close values of μ_{tot} and μ_{sat} at low temperatures.

In these devices, a good knowledge of the hole concentration in p-type GaAs buffer layer is required in order to model and optimize the device structure for high performance operation. Therefore, van der Pauw measurements were performed in the selectively etched device. All the n-type layers were removed down to the p-type GaAs buffer layer by selective etching in $H_2SO_4:H_2O_2:H_2O$ solution with 4:1:50 ratio. InZn (4% of Zn) was used as a p-type contact. Van der Pauw measurements were carried out in the lattice temperature range between 20 and 300 K. The result is shown in Fig. 5. It is evident from this figure that the temperature behaviour of the hole density

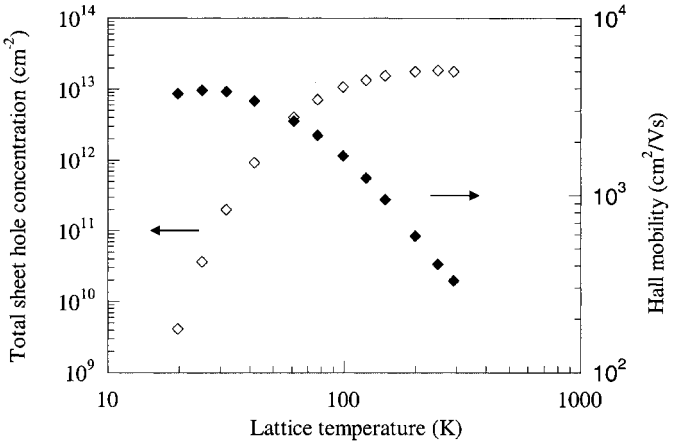

Fig. 5. Hole concentration and mobility as a function of lattice temperature for sample ES1

shows clearly the bulk nature of holes. At high temperatures, most of the acceptors are ionized and hence hole concentration tends to saturate. As the temperature decreases sheet hole density freezes out. In order to obtain the 3D hole concentration, the sheet hole concentration obtained at T_L = 300 K was simply divided by the thickness of the GaAs buffer layer. We obtained a 3D hole of $p_{3D} = 4.6 \times 10^{16}$ cm^{-3} for sample ES1. This value is in good agreement with the value given in the growth menu, $p_{3D} = 5.0 \times 10^{16}$ cm^{-3}. The difference may be due to the overestimation of the layer thickness. The temperature dependence of the hole density allows us to evaluate the thermal ionization energy of acceptors, which would help us in interpreting the photoluminescence peak energies [1, 2]. The dependence of the hole density on temperature with acceptor activation energy E_a is given by [10]

$$p_{2D} \propto \exp\left(-\frac{E_a}{2k_B T_L}\right). \tag{2}$$

Therefore, the logarithm of hole density plotted as a function of inverse lattice temperature gives the acceptor ionization energy. This is shown in Fig. 6 where the acceptor

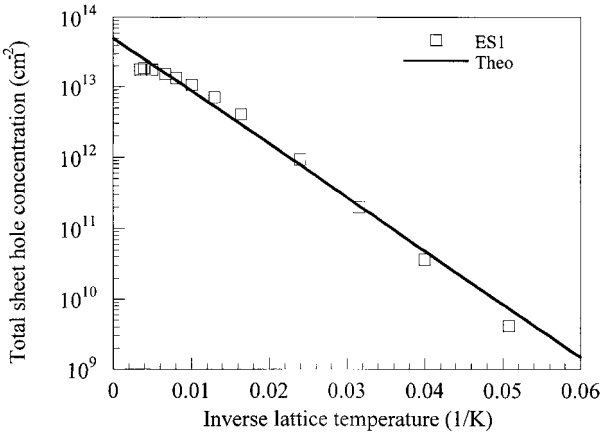

Fig. 6. Logarithmic plot of 2D hole concentration versus inverse lattice temperature for sample ES1. The solid line is an exponential fit of the experimental points

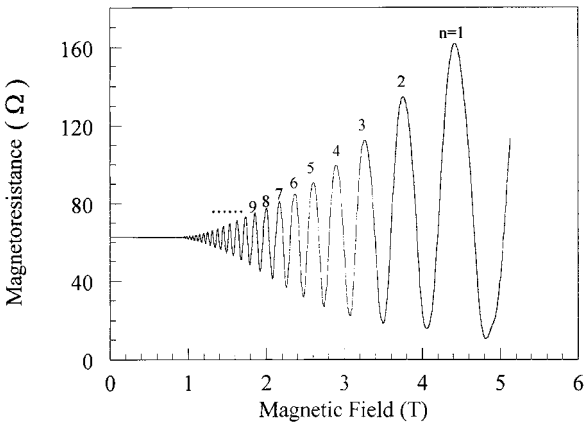

Fig. 7. Magnetoresistance oscillations versus magnetic field at T_L = 1.5 K. The numbers are the oscillation peak numbers n = 1, 2, 3, 4, ...

ionization energy of E_a = 30 meV is in good agreement with the value for Be acceptors in GaAs [10].

As we mentioned before, Hall measurements only provide information about the total sheet carrier concentration n_{Hall} and Hall mobility μ_{Hall}. To evaluate the 2D electron concentration per well n_{2D} at the Fermi level and quantum mobility μ_q, we have used SdH results. Typical magneto-resistance oscillations observed in sample ES1 are shown in Fig. 7. The 2D electron density per well can be obtained from the plots of the reciprocal magnetic field ($1/B_n$), at which the n peaks occur, against the peak number (n). Figure 8 shows the peak number n versus $1/B_n$ (the data were taken at each maximum peak). Since only the first subband is populated the graph gives a straight line as seen in Fig. 8. The 2D electron density can now be calculated from the slope of the figure. The quantum mobility μ_q of 2D electrons can also be calculated by analysis of the SdH oscillations. Details of this calculation can be found in Refs. [11] and [12]. The results for n_{2D} and μ_q are shown in Table 1 together with the results of n_{Hall} and μ_{Hall} obtained from Hall measurements for samples ES1 and ES2.

The sample ES1 has ten identical quantum wells (see Fig. 1). Therefore, the ratio of the total sheet carrier density to the 2D electron density per well (n_{Hall}/n_{2D}) should

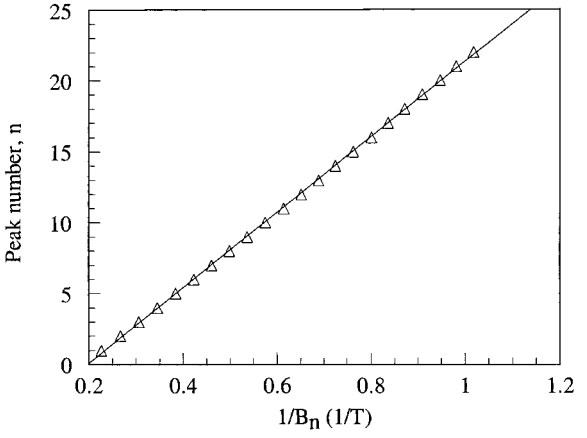

Fig. 8. Oscillation peak number n versus reciprocal magnetic field. The open circles correspond to experimental data, the straight line is the best fit to experimental data

Table 1

The 2D carrier density n_{2D} and quantum mobility μ_{2D} obtained from SdH measurements, and total sheet carrier density n_{Hall} and Hall mobility μ_{Hall} obtained from Hall measurements for samples ES1 and ES2

sample	n_{2D} (10^{12} cm^{-2})	n_{Hall} (10^{12} cm^{-2})	n_{Hall}/n_{2D}	μ_q (m^2 V^{-1} s^{-1})	μ_{Hall} (m^2 V^{-1} s^{-1})	μ_q/μ_{Hall}
ES1	1.24	10.2	8.23	0.86	3.95	0.22
ES2	1.08	11.5	10.6	0.88	2.88	0.30

give the number of quantum wells which is ten for ES1 if it is assumed that there is no parallel conduction and no depletion in the quantum wells. From Table 1 it is evident that the ratio $n_{Hall}/n_{2D} = 8.23$. This shows that some of the quantum wells are depleted for ES1. The sample ES2 has also ten identical quantum wells, which contribute to the total conduction (see Fig. 1). However, from the theoretical calculation [1, 2], there is a finite electron density in the inversion layer in equilibrium. Therefore, the n_{Hall}/n_{2D} ratio should be 11 for this sample (ES2). From Table 1 it is seen that the ratio $n_{Hall}/n_{2D} = 10.6$, which is very close to the expected value of 11. Therefore, one of the quantum wells might be depleted in this sample. It is also evident from the results discussed above that there are no significant parallel conduction channels neither in the $Al_{0.33}Ga_{0.67}As$ barriers nor in the p-type buffer layer which contributes to the major conduction in the quantum wells.

The ratio of the quantum mobility and Hall mobility μ_q/μ_{Hall}, which depends on the mean scattering angle, gives information about the dominant scattering mechanism. It has been reported in GaAs/$Al_xGa_{1-x}As$ heterostructures that the ratio μ_q/μ_{Hall} is less than unity if small-angle scattering, such as remote ionized impurities or background impurity scattering, dominates. The ratio μ_q/μ_{Hall} is equal or greater than unity if wide-angle scattering, such as interface roughness, dominates [13]. In our samples, the ratio of quantum mobility to Hall mobility, μ_q/μ_{Hall}, is less than unity. In Ref. [13], the authors obtained a μ_q/μ_{Hall} ratio in the range of 0.1 for small-angle scattering. The ratios μ_q/μ_{Hall} for ES1 and ES2 are larger than 0.1 and less than unity, therefore, the results indicate that the scattering mechanisms limiting the electron mobilities in our samples is determined by the combi-

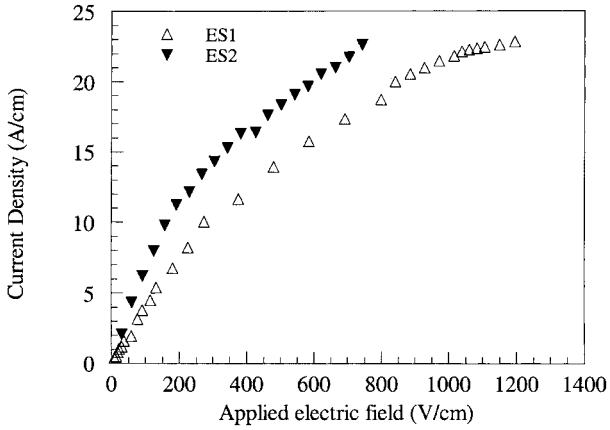

Fig. 9. Current density versus applied electric field for ES1 and ES2 at $T_L = 77$ K

nation of both interface roughness and background impurity scattering arising from dopant (Si) segregation from the doped $Al_xGa_{1-x}As$ into the GaAs quantum well interface.

In the measurements of electrical transport (Hall and SdH measurements) discussed so far, the electric field was limited to less than several V/cm. Here, we present the high-field characterization of the samples studied, high-speed I–V measurements in the lattice temperature range of 77 to 300 K. In these measurements, simple bar geometry with dimensions of 4.3×1.03 and 2.5×0.68 mm^2 were used for samples ES1 and ES2, respectively. Typical results are shown in Fig. 9. The data shown in this figure were obtained at $T_L = 77$ K. The current density was calculated by dividing the current by the width of the samples and the electric field was obtained by dividing the voltage by the length of the samples.

Both samples show Ohmic behaviour up to applied electric fields of $F \sim 100$ V/cm. At fields greater than $F \sim 100$ V/cm the current density versus applied electric field characteristics show a sublinear behaviour as expected from the electron heating and hence enhanced electron–LO phonon scattering [14]. Deviation from Ohm's law at high fields can also clearly be seen from Figs. 10a and b, where the electron mobility

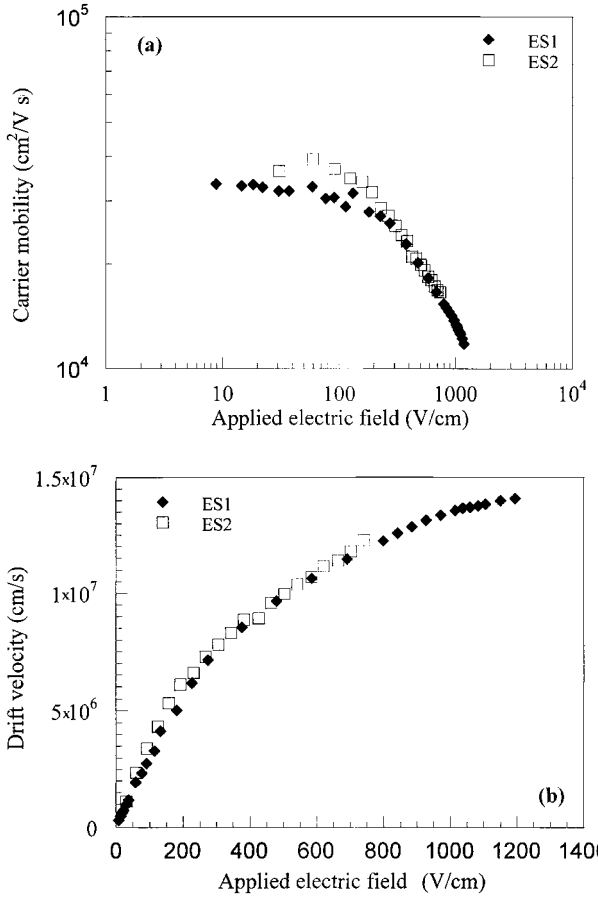

Fig. 10. a) Carrier mobility and b) drift velocity versus applied electric field at lattice temperature of 77 K for the samples ES1 and ES2

and drift velocity are plotted as a function of applied electric field, respectively. In Fig. 10a, at low fields (up to an applied electric field $F \sim 100$ V/cm), where the I–V characteristic shows Ohmic behaviour, the electron mobilities are almost constant. At above $F \sim 100$ V/cm the mobility decreases with increasing field due to the enhanced LO phonon scattering. It is also evident from Fig. 10b that electron drift velocities show a linear dependence on applied electric field up to $F \sim 100$ V/cm. Then they increase with applied field sublinearly tending to saturate at the highest applied field. The estimated saturation drift velocity for all the samples is almost the same, V_d (saturation) = 1.5×10^7 cm/s, as expected for the GaAs/$Al_xGa_{1-x}As$ quantum well system at 77 K [15].

4. Discussion and Conclusions

The electrical characterization of HELLISH-2 was performed at low and high electric and magnetic fields. Total sheet electron densities and mobilities of the samples were determined by using standard Hall measurements. All the samples have shown almost the same temperature behaviour. SdH results coupled with Hall data were used to determine parallel conduction effects and scattering mechanisms at low lattice temperatures for samples ES1 and ES2. It has been found out that the dominant scattering mechanisms for both samples are interface roughness and background impurity scattering, and optical phonon scattering at low and high lattice temperatures, respectively. There was no parallel conduction observed for ES1, and a small parallel conduction was realized in $Ga_{1-x}Al_xAs$ barrier for sample ES2. Hall measurements were also performed on selectively isolated p-type GaAs buffer layers to determine 3D hole density and acceptor ionization energy. The contribution of the p-layer to the total conductivity was negligible at low temperatures. The electrical characterization at high electric fields was carried out by using high-speed I–V measurement techniques. Current density and drift velocity at high fields were measured. The nonlinear behaviour of both is shown to be due to electron heating and therefore, to enhanced LO phonon scattering.

In conclusion, we have demonstrated an electrical analysis of a longitudinally biased light emitting device, which was recently developed by us, using standard measurement techniques. Since HELLISH-2 devices have shown some advantages over conventional light emitters for using some potential application, such as optical logic gates, tunable wavelength light emitter and VCSEL in optoelectronic technology [1, 2], it is important to understand the operation principle and to optimize the structure for higher performance. The device structure can be optimized for low threshold and high intensity output. This can be achieved by increasing the phonon-assisted tunnelling current while the thermionic emission current is kept constant by changing the structural parameters. Two parameters play an important role in determining the phonon-assisted tunnelling current. The first one is the energy separation between the quantum well and the inversion layer first subbands, which should be close to the optical phonon energy $(\hbar\omega)_{LO}$. The second one is the barrier width that should be reduced to increase hot electron tunnelling currents from quantum well to the inversion layer. Energy separation between the first subbands in the quantum well and in the inversion layer can be altered simply by changing the p-doping density in the GaAs buffer layer. It is also possible to meet the first condition by changing the quantum well width adjacent to the junction plane. For the second condition we can simply reduce the barrier width between quantum well and inversion layer. Therefore, a good knowledge of these electrical param-

eters obtained in this work helped us to analyze the luminescence results in detail and optimize the structure for low threshold and higher performance operation according to our model.

Acknowledgement The author would like to thank Dr. N. Balkan, Electronic System Engineering of Essex University, UK for his support and valuable discussion.

References

[1] N. Balkan, A. Teke, R. Gupta, A. Straw, J. H. Wolter, and W. van der Vleuten, Appl. Phys. Lett. **67**, 935 (1995).
[2] A. Teke, R. Gupta, N. Balkan, J. H. Wolter, and W. van der Vleuten, Semicond. Sci. Technol. **12**, 314 (1997).
[3] P. Blood and J. W. Orton, The Electrical Characterization of Semiconductors: Majority Carriers and Electron States, Academic Press, 1992.
[4] E. E. Mendez, P. J. Price, and M. Heiblum, Appl. Phys. Lett. **45**, 294 (1984).
[5] B. J. F. Lin, D. C. Tsui, M. A. Paalanen, and A. Gossard, Appl. Phys. Lett. **45**, 965 (1984).
[6] T. Ishikawa, J. Saito, S. Sasa, and S. Hiyamizu, Jpn. J. Appl. Phys. **21**, l675 (1982).
[7] H. Sakaki, T. Noda, K. Hirakawa, M. Tanaka, and T. Matsusue, Appl. Phys. Lett. **51**, 1934 (1987).
[8] J. J. Harris, R. B. Beall, J. B. Clegg, C. T. Foxon, S. J. Battersby, D. E. Lacklison, G. Duggan, and C. M. Hellon, J. Cryst. Growth **95**, 257 (1989).
[9] W. Walukievizc, H. E. Ruda, J. Lagowski, and H. C. Gatos, Phys. Rev. B **30**, 4571 (1984).
[10] S. M. Sze, Physics of Semiconductor Devices, 2nd ed., Wiley, New York 1981.
[11] N. Balkan, H. Çelik, A. J. Vickers, and M. Cankurtaran, Phys. Rev. B **52**, 17210 (1995).
[12] H. Çelik, M. Cankurtaran, A. Bayrakli, E. Tiras, and N. Balkan, Semicond. Sci. Technol. **12**, 389 (1997).
[13] J. P. Harrang, R. J. Higgins, R. K. Goodall, P. R. Jay, M. Laviron, and P. Delescluse, Phys. Rev. B **32**, 8126 (1985).
[14] J. Shah, IEEE J. Quantum Electron. **22**, 1728 (1986).
[15] R. Gupta, N. Balkan, and B. K. Ridley, Semicond. Sci. Technol. **7**, 274 (1992).